Absorption Induced by Mn Doping of ZnS for Improved Sensitized Quantum-Dot Solar Cells

S. Horoz, Q. Dai, F. S. Maloney, B. Yakami, J. M. Pikal, X. Zhang, J. Wang, W. Wang, and J. Tang

Phys. Rev. Applied **3**, 024011 — Published 23 February 2015

DOI: 10.1103/PhysRevApplied.3.024011

Mn doping induced absorption in ZnS for improved quantum dot sensitized solar cells

S. Horoz,[1] Q. Dai,[1] F.S. Maloney,[1] B. Yakami,[2] J.M. Pikal,[2] X. Zhang,[3]

J. Wang,[3] W. Wang[1] and J. Tang[1*]

[1]Department of Physics and Astronomy, University of Wyoming, Laramie, WY 82071

[2]Department of Electrical Engineering, University of Wyoming, Laramie, WY 82071

[3]Ministry of Education Key Laboratory of Bioinorganic and Synthetic Chemistry, State Key Laboratory of Optoelectronic Materials and Technologies, School of Chemistry and Chemical Engineering, Sun Yat-sen University, Guangzhou, 510275, China

[*]Contact: jtang2@uwyo.edu

ABSTRACT

ZnS quantum dots (QDs) have limited application potential in QD sensitized solar cells because of their wide band gap, which does not allow absorption of sunlight in the visible and infrared regions. Introducing intermediate energy levels in the QDs is one way to expand the absorption window into the visible region. We show that this effect is achieved in Mn doped ZnS QDs. Mn doped ZnS QDs were synthesized by laser ablation in water and solution-based method. The structural, optical, and magnetic properties of the ZnS:Mn QDs have been examined by x-ray diffraction (XRD), transmission electron microscope (TEM), photoluminescence emission (PL) and excitation (PLE), and magnetic susceptibility measurements. The average particle size of cubic phase ZnS:Mn estimated from the XRD and TEM is about 3 nm. The QDs show two PL peaks near 450 nm and 600 nm, which are attributed to the defect related emission of ZnS and emission of Mn^{2+} in a ZnS host, respectively. The PLE spectra exhibit near band edge absorption of ZnS at 350 nm and the absorption of Mn^{2+} internal energy levels around 468 nm. The latter is due to the transitions of the $3d^5$ electronic states of Mn^{2+} from the ground state $^6A_1$ to excited states $^4A_1$ and ^4E and plays an important role in improving the absorption of the material in the visible region. ZnS:Mn QDs coated on Zn_2SnO_4 nanowires show greatly improved sensitization in the visible region as demonstrated by incident photon to electron conversion efficiency experiments. Our study also shows that the characteristics of the solar cells performance can be tuned with the Mn concentration.

INTRODUCTION

Over the years, much attention has been paid to Mn-doped ZnS semiconductors and quantum dots (QDs) for their novel optical properties (1-7). The optical properties of these materials can be tuned owing to quantum confinement effect, which leads to size-dependent band gap energy in QDs and is the basis for QD sensitized solar cell technology (8). Bulk ZnS has a wide band-gap energy of 3.68 eV, which limits its ability to absorb visible light (9-12). ZnS QDs have even wider band gaps than the bulk and are unsuitable for QD sensitized solar cell applications. Since ZnS is an environmentally benign and earth abundant material, it is desirable to find means to modify its energy levels such that it becomes a good absorber of solar energy. One way to approach this is by introducing intermediate energy levels in the band gap through doping. The intermediate/impurity states can significantly change the electronic structure and transitions among various energy levels (1). The doped Mn^{2+} ions act as recombination centers for the excited electron-hole pairs due to strong interactions of its 3d electrons with the s-p electrons of the ZnS hosts and show characteristic orange luminescence (13). The orange luminescence near 590 nm is attributed to the spin forbidden $^4T_1$-$^6A_1$ transition of the 3d states of Mn^{2+} on the substitutional Zn sites, where Mn^{2+} is coordinated by four S^{2-} nearest neighbors (14, 15). At higher Mn concentrations, this orange luminescence becomes progressively quenched, which gives rise to a red emission band (16). Although the origin of the red emission band is not well understood, the concentration quenching is most likely due to dipole-dipole interaction or exchange coupling between the Mn^{2+} ions (17). It may also be facilitated by trapped states like those formed on the surfaces of the QDs (18). It is of both fundamental and technological interest to explore these effects for QD sensitized solar cells as the increased overlap between the wave functions and coupling among various centers in a QD may lead to either enhancement or

quenching of the luminescence (19). The lifetimes of the relevant excited states can be altered by these interactions and also by spin selection rules in the magnetically doped ZnS, which may be another way to control the photovoltaic characteristics, in addition to tuning the absorption windows.

In addition to solution based methods, there are several ways to make QDs using deposition-based methods such as successive ionic layer adsorption and reaction (SILAR), chemical bath deposition (CBD), and atomic layer deposition (ALD) (see references in 20-21). In recent years, the preparation of nanoparticles using laser ablation in liquids has been explored (22-25) although this method has been studied to a much lesser extent for QD synthesis (26-28). In our previous study, we have succeeded in QD preparation in a one-step synthesis process using pulsed laser ablation in liquid (20).

In this work, we report the properties of Mn doped ZnS QDs prepared by laser ablation in water as well as by a solution based method. The as-prepared the ZnS:Mn QDs were subsequently used to make ligand-free QD sensitized Zn_2SnO_4 nanowire solar cells. Incident photon to electron conversion efficiency (IPCE) measurements show improved performance in the visible region for the doped samples, consistent with enhanced absorption seen in the photoluminescence excitation spectra.

EXPERIMENTAL

ZnS:Mn QDs with various doping concentration (0 – 5 %) have been synthesized by both wet chemical co-precipitation method and pulsed laser ablation in water. Appropriate amounts of $Zn(CH_3COO)_2 \cdot 2H_2O$ and $Mn(CH_3COO)_2 \cdot 2H_2O$ were dissolved in deionized water with stirring at room temperature. Deionized water solution of Na_2S was then added to the above

solution with vigorous stirring. The resulting white precipitate was collected through a filter paper, centrifuged and washed with water and ethanol. The precipitate was dried at 120 ^{o}C overnight. To obtain the target for pulsed laser ablation, the white powders were pressed into a pellet and annealed at 900 ^{o}C for 8 hrs. A YAG:Nd laser (wavelength: 266 nm) with a repetition rate of 10 Hz was used in the experiment. The laser beam was focused by a lens with focal length of 5 cm, which was placed immediately in front of a fused quartz bowl, onto a ZnS:Mn target submerged in deionized water inside of the bowl. The laser fluence of 1 J/cm^2 on the ZnS:Mn target surface was applied. The laser ablation was carried out for several hours for enough samples to be collected from the water.

The samples were characterized with x-ray diffraction (XRD) by dropping QD solution onto clean silicon substrate and drying at room temperature. Transmission electron microscopy (TEM) images of ZnS:Mn QDs dropped on carbon-coated copper grids were obtained with a FEI Tecnai G2 F20 TEM operated at an acceleration voltage of 200 kV. Photoluminescence (PL) measurements were performed at room temperature with a tunable femtosecond laser as the excitation source and the PL was collected through a ½ m scanning monochromator using a high gain Si detector and lock-in amplifier locked to the laser repetition rate. The photoluminescence excitation (PLE) spectra were determined at room temperature on a FSP920-combined Time Resolved and Steady State Fluorescence Spectrometer (Edinburgh Instruments), equipped with a 450 W Xe lamp, TM300 excitation monochromator, double TM300 emission monochromators and thermo-electric cooled red sensitive PMT. The spectral resolution is about 0.05 nm in UV-VIS.

Zn_2SnO_4 nanowires were synthesized on gold-coated (3 nm) Si substrates following a procedure published elsewhere (29). This process was able to reliably reproduce nanowire films

of roughly 20 μm thick. The nanowires were then transferred to FTO substrates following a printing procedure (29) and annealed at 500°C for 4 hours to transform the precursor on FTO into a Zn_2SnO_4 film.

The annealed FTO substrates with the nanowires were placed in a suspension of ZnS:Mn QDs in water and allowed to soak for 24 hours. Immediately upon removal from the QD suspension, the substrates were dried with N_2 gas and secured against a Cu_2S counter electrode containing a polysulfide electrolyte (0.25 M Na_2S and 0.1 M NaOH in 18 MΩ water). Cu_2S counter electrodes were fabricated following a procedure published elsewhere (21). IPCE was measured immediately after device fabrication. Data was obtained using a monochromatic light source consisting of a 50 W tungsten halogen lamp and a monochromator. The light beam was modulated by a chopper and a lock-in amplifier (Stanford Research SR830). All measurements were made in the dark. Magnetic susceptibility of the QDs was measured on a physical property measurement system (PPMS) from Quantum Design.

RESULTS AND DISCUSSION

We have found that samples made with both methods are of similar average particle size (about 3 nm). And both methods are effective in doping Mn into the ZnS QDs. Figure 1a and 1b are the TEM image and particle size distribution, respectively, of ZnS:Mn (3 at.%) QDs prepared by laser ablation in water. The Mn concentration was determined with energy dispersive x-ray spectroscopy (EDS) and magnetic susceptibility measurements. The particle size distribution was obtained by measuring the diameter of 100 particles from representative TEM images. The particles are nearly spherical and the size distribution is reasonably narrow with a mean diameter of 2.9 nm. An XRD pattern of the QDs is shown in Fig. 2. All peaks of ZnS:Mn QDs can be

identified as those of Zinc Blende ZnS. The three diffraction peaks are positioned at $2\theta = 28.5°$, 48.3°, and 56.3° and correspond to the (111), (220), and (311) planes, respectively, of the cubic ZnS. No peaks corresponding to Mn compounds or oxides were observed. The average size of the ZnS:Mn QDs, estimated from the full width at half height of diffraction peaks using Debye–Scherrer formula, is 2.8 nm. This result is in agreement with that from the TEM images.

All doped samples show paramagnetic behavior. The magnetic susceptibility as a function of temperature for the ZnS:Mn (3 at.%) measured with a PPMS is shown in Fig. 3. The inverse of the magnetic susceptibility versus temperature is shown in the inset. From a linear fit of the experimental data to the Curie-Weiss law, a paramagnetic Curie temperature of $\theta = -3.2$ K is obtained, suggesting antiferromagnetic interaction between the Mn moments in the QDs. The Curie constant obtained from the linear fit shows that the Mn^{2+} concentration of the sample is indeed 3%. The paramagnetic Curie temperature θ is negative for all samples and its magnitude increases with the Mn concentration, consistent with increased antiferromagnetic coupling between the Mn moments. At 5 at.%, $\theta = -5.3$ K.

Figure 4 shows the room temperature PL spectra of ZnS:Mn QDs with excitation wavelength $\lambda = 310$ nm. The spectra were taken on QDs suspended in methanol since it was difficult to get PL signals in water suspension. The plots are normalized to the broad peak near 450 nm. This wide blue band around 400-500 nm is typical of ZnS resulting from radiative recombination due to the presence of surface defects and Zn/S vacancies (30, 31). The PL spectra show a second peak near 600 nm. As mentioned in the Introduction, this is a characteristic emission of Mn^{2+} ions in ZnS and associated with the internal $^4T_1$ - $^6A_1$ transition. It is also a proof that the Mn^{2+} substitutes for Zn^{2+} in the ZnS lattice. Its intensity relative to that at 450 nm increases with the Mn concentration as expected. Since it is known that the presence

of Mn^{2+} on the surface of ZnS nanoparticles stabilizes near band edge emission in the ultraviolet region (30), the absence of the PL peak near 350 nm is a further evidence that the Mn dopants are distributed inside the ZnS QDs, instead of on the surfaces.

The absorption spectra of three ZnS:Mn samples (0, 0.5 and 5 at.%) are shown in the inset of Fig. 5. All samples show absorption peaks due to the band edge absorption around 300 nm, which is consistent with quantum confinement effect on the band gap of ZnS QDs. The average particle size determined from the peak position of the 0.5 at.% sample is about 3.2 nm (32). The slight difference in the peak position of the samples is due to their size difference and not due to the Mn concentration. The PLE spectrum of the 0.5 at.% QDs is shown in Fig. 5. The PLE measurement was monitored at 610 nm. A strong peak appears near 350 nm and is due to the excitations from the ZnS QD host (3, 30) that is followed by energy transfer to the Mn. It is known that the PLE peak of the nanoparticles is located at the longer wavelength side of the absorption band, because the excitation is concentrated around the absorption edge where the absorption index is fairly low and the dispersion small (33,34). The strong main peak near 350 nm is accompanied by a small shoulder at 300 nm. The nature of the shoulder is not well understood at present. There are reports claiming that the shoulder may be due to particle size distribution (35), absorption by high level excited Mn^{2+} internal states (33), or organic molecules/polymers capping the ZnS QDs (36). We can rule out the last as a possible mechanism from the way the samples were prepared, in which there was no organic molecules involved.

Figure 5 shows, in addition, a weak peak at 468 nm, which is attributed to the excitation transition of the $3d^5$ electrons from the ground state $^6A_1$ to the excited states $^4A_1$ and ^4E (37). This excitation peak is often missed in PLE measurements due to the emissions that occur at

about the same wavelengths. However, its presence is well established here and elsewhere (3,33) and plays a critical role in enriching the absorption window of our solar cells as will be discussed below. Although not obviously seen in Fig. 5 due to the relatively weak signals, the excitations from the ground state $^6A_1$ to $^4T_2(^4D)$ (λ = 430 nm), to $^4T_2(^4G)$ (λ = 498 nm), and to $^4T_1$ (λ = 535 nm) (38), which are typically observed together with the one at λ = 468 nm, should also contribute to the enhanced absorption in the solar cells. A representative schematic diagram of the energy levels is shown in Figure 6. The band gap and energy levels of the conduction band (CB) and valence band (VB) edges of ZnS are adopted from Ref. 39 and adjusted for particle size of 3.2 nm (32). The positions of the energy levels of the crystal-field-split internal Mn^{2+} states relative to that of ZnS are not precisely known. It also depends on which model, local internal Mn^{2+} states versus 3d bands formed by the Mn electrons (40), is used. We have adopted the former in this paper as it is appropriate to describe the PL/PLE spectra. The estimated positions shown in Fig. 6 are derived from the available literature (30,40,41) and consistent with the experiments including those presented here. It represents the best depiction of the energy levels of Mn doped ZnS to date. We have also included the energy levels of the CB and VB edges of Zn_2SnO_4 anode (21). The energy levels of the defect states of ZnS are not the focus of this study, and their relative positions in ZnS are only for illustration and should not be considered accurate.

Figure 7 shows the IPCE spectra of ligand-free ZnS:Mn QDs of various doping concentrations coated on Zn_2SnO_4 nanowires. One of the most important results of this investigation is that the onset wavelength of the Mn doped samples is significantly red shifted. While the undoped sample does not have much IPCE intensity for λ > 400 nm, the onset of IPCE for the doped QDs occurs near 550 nm. This is consistent with the PLE data of ZnS:Mn

discussed above. Keep in mind the excitation wavelength from the ground state $^6A_1$ to the first excited state $^4T_1$ is λ = 535 nm. At the wavelength of 400 nm, the IPCE value increases from 0.18 % of the undoped sample to 0.85 % for the sample doped with 0.5 at.% Mn. It further increases to 2.25 % at 3 at.% Mn doping. The process can be understood with the aid of Fig. 6 as follows. For the undoped ZnS, the absorption occurs mainly for $\lambda < 300$ nm. The Mn doping widens the absorption window to longer wavelengths due to the addition of the Mn^{2+} internal energy levels. Electrons photoexcited to the various excited states of Mn^{2+} can be injected into the Zn_2SnO_4 electrode because their energy levels are all higher than the CB edge of Zn_2SnO_4. Note, the injection can go via two possible routes, either directly from the respective excited states where the electrons are excited to, or from the first excited state $^4T_1$ after the photoexcited electrons relax to $^4T_1$.

Upon further increasing the Mn concentration to 5 at.%, the IPCE efficiency increases to 4.5 % at 400 nm. However, the efficiency decreases at longer wavelengths (see Fig. 7). The IPCE values for $\lambda > 465$ nm is lower than both 0.5 and 3 at.%. The reason is given below. At high enough Mn doping level, concentration quenching of the luminescence occurs. In fact, concentration quenching of the 600 nm emission is known to occur and is accompanied by the appearance of a red emission band at about 700-720 nm (16). Indeed, we have observed the red emission band at 700 nm in the 5 at.% sample as shown in the inset of Fig. 7, which is not seen in the two samples doped at lower Mn concentrations. This suggests a pathway for the excited electrons in $^4T_1$ state to recombine radiatively with the holes via the states related to the red emission, which leads to reduced injection of electrons from $^4T_1$ to the Zn_2SnO_4 conduction band. Although the nature of the 3d states related to the red emission is not well understood, several possible mechanisms may be responsible for the concentration quenching, i.e., dipole-

dipole interaction, exchange coupling between the Mn^{2+} ions, or via trapped states like those formed on the surfaces of the QDs (17-18). Noticing the high IPCE efficiency of the 5 at.% sample from 400 to 450 nm, the electron injection from the higher excited states of the Mn^{2+} internal levels (e.g., $^4A_1$, ^4E and $^4T_2(^4D)$) should not be affected by the concentration quenching, rather the high level of Mn doping results in the high efficiency. Our data do not allow us to make assessment on whether the IPCE enhancement over this wavelength region is purely due to high Mn content or impacted by exchange coupling between Mn^{2+} ions. It remains an interesting subject to be investigated further.

CONCLUSIONS

In this study, ZnS:Mn QDs have been investigated for QD sensitized photovoltaic solar cells. Structural, optical and magnetic properties of the ZnS:Mn QDs suggest Mn^{2+} ions substitute for Zn in cubic ZnS and produce characteristic orange emission near 600 nm. The ZnS:Mn QDs have been attached to Zn_2SnO_4 nanowires without ligand molecules to make QD sensitized solar cells. IPCE measurements show that the conversation efficiency is improved due to widened absorption window into the visible region, which are shown to benefit from the transitions between Mn^{2+} internal energy levels. The wavelength dependence of the solar cells performance can be tuned with the Mn concentration via the interactions between the Mn^{2+} ions. Our study suggests that introducing intermediate energy levels in wide band gap QDs is an effective method to expand the absorption window into the visible region to improve the device performance of QD sensitized solar cells.

Acknowledgement:

This work was supported by the U.S. Department of Energy, Office of Basic Energy Sciences, Division of Materials Sciences and Engineering under Award DE-FG02-10ER46728.

REFERENCES:

(1) P. K. Santra and P. V. Kamat, Mn-doped quantum dot sensitized solar cells: a strategy to boost efficiency over 5%, J. Am. Chem. Soc., **134**, 2508 (2012)

(2) H.-E. Gumlich, Electro- and photoluminescence properties of Mn^{2+} in ZnS and ZnCdS, J. Luminescence, 23, 73 (1981)

(3) W. Q. Peng, S. C. Qu, G. W. Cong, X. Q. Zhang, Z. G. Wang, Optical and magnetic properties of ZnS nanoparticles doped with Mn^{2+}, J. Crystal Growth, **282,** 185 (2005)

(4) S. W. Lu, B. I. Lee, Z. L. Wang, W. Tong, B. K. Wagner, W. Park, C. J. Summers, Synthesis and Photoluminescence Enhancement of Mn Doped ZnS Nanocrystals, J. Luminescence, **92**, 73 (2001)

(5) D.S. McClure, The Optical Spectra of Exchange Coupled Mn++ Ion Pairs in ZnS:MnS, J. Chem. Phys., **39**, 2850 (1963)

(6) H. Yang, P.H. Holloway, B.B. Ratna, Photoluminescent and electroluminescent properties of Mn-doped ZnS nanocrystals, J. Appl. Phys. **93**, 586 (2003)

(7) A. D. Dinsmore, D. S. Hsu, H. F. Gray, S. B. Qadri, Y. Tian and B. R. Ratna, Mn-doped ZnS nanoparticles as efficient low-voltage cathodoluminescent phosphors, Appl. Phys. Lett. **75**, 802 (1999)

(8) A. J. Nozik, Quantum dot solar cells, Physica E, **14,** 115 (2002)

(9) P. Yang, M. Lu, D. Xu, D. Yuan, C. Song, G. Zhou, Photoluminescence properties of ZnS nanoparticles co-doped with Pb^{2+} and Cu^{2+}, Chem. Phys. Lett., **336**, 78 (2001)

(10) H. Hu, W. Zhang, Synthesis and properties of transition metals and rare-earth metals doped ZnS nanoparticles, Optical Materials, **28,** 550 (2006)

(11) Y. Q. Li, J. A. Zapien, Y. Y. Shan, Y. K. Liu, S. T. Lee, Manganese doping and optical properties of ZnS nanoribbons by postannealing, Appl. Phys. Lett., **88** , 013115 (2006)

(12) H. Y. Xu, Y. C. Liu, C. S. Xu, Y. X. Liu, C. L. Shao *et al.*, Structural, optical, and magnetic properties of Mn-doped ZnO thin film, J. Chem. Phys., **124**, 074707 (2006)

(13) R.N. Bhargava, D Gallagher, X. Hong, A. Nurmikko, Optical proeprties of Manganese doped Nanocrystals of ZnS, Phys. Rev. Lett., **72**, 416 (1994)

(14) M. A. Malik, P. O'Brien, N. Revaprasadu, Synthesis of TOPOcapped Mn-doped ZnS and CdS quantum dots, J. Materials, **11**, 1039 (2001)

(15) Bian, W., Ma, J., Liu, Q., Wei, Y., Li, Y., Dong, C., Shuang, S, A novel phosphorescence sensor for Co2+ ion based on Mn-doped ZnS quantum dots, Luminescence, **7,** 151 (2013)

(16) M. D. Bhise, M. Katiyar, A. H. Kitai, Effect of Mn concentration on the cathodo- and photoluminescence of ZnS:Mn, J. Appl. Phys., **67,** 1492 (1990)

(17) P. H. Borse, D. Srivinas, R. F. Shinde, S. K. Date, W. Vogal, and S. K. Kulkarni, Effect of Mn^{2+} concentration in ZnS nanoparticles on photoluminescence and electron-spin-resonance spectra, Phys. Rev. B, **60**, 8659 (1999)

(18) M. Katiyar and A. H. Kitai, Luminescence concentration quenching due to energy migration in ZnS: Mn with fixed trap density, J. Luminescence, **46**, 227 (1990)

(19) K. T. Al- Rasoul, N. K. Abbas, Z. J. Shanan, New method of preparation ZnS Nano size at low pH, Int. J. Electrochem. Sci., **8**, (2013)

(20) S. Horoz, L. Liyou, Q. Dai, J. Chen, B. Yakami *et al*., CdSe quantum dots synthesized by laser ablation in water and their photovoltaic applications, Appl. Phys. Lett., **101**, 223902 (2012)

(21) Q. Dai, J. Chen, L. Liu, J. Tang, W. Wang, Pulsed Laser Deposition of CdSe Quantum Dots on Zn_2SnO_4 Nanowires and Their Photovoltaic Applications, Nano Letters, **12**, 1021 (2012)

(22) H. Zeng, X. W. Du, S. C. Singh, S. A. Kulinich, S. Yang, J. He, and W. Cai, Nanomaterials via laser ablation/irradiation in liquid: a review, Adv. Funct. Mater. **22**, 1333 (2012).

(23) N. G. Semaltianos, Nanoparticles by Laser Ablation, Crit. Rev. Solid State Mater. Sci., **35**, 105 (2010).

(24) Z. Yan and D. B. Chrisey, Pulsed Laser Ablation in Liquid for Micro-/Nanostructure Generation, J. Photochem. Photobiol. C: Photochem. Rev., **13**, 204 (2012).

(25) A. V. Simakin, V. V. Voronov, N. A. Kirichenko, and G. A. Shafeev, Nanoparticles Produced by Laser Ablation of Solids in Liquid Environment, Appl. Phys. A, **791**, 1127 (2004).

(26) K. V. Anikin, N. N. Melnik, A. V. Simakin, G. A. Shafeev, V. V. Voronov, and A. G. Vitukhnovsky, Formation of ZnSe and CdS quantum dots via laser ablation in liquids, Chem. Phys. Lett., **366**, 357 (2002).

(27) N. G. Semaltianos, S. Logosthetidis, W. Perrie, S. Romani, R. J. Potter, M. Sharp, P. French, G. Dearden, and K. G. Watkins, CdSe nanoparticles synthesized by laser ablation, Europhys. Lett. , **84**, 47001 (2008).

(28) A. A. Ruth and J. A. Young, Generation of CdSe and CdTe nanoparticles by laser ablation in liquids, Colloids Surf. A: Physicochem. Eng. Aspects, **279**, 121 (2006).

(29) J. Chen, L. Lu, W. Wang, Zn2SnO4 nanowires as photoanode for dye-sensitized solar cells and the improvement on open-circuit voltage, J. of Phys. Chem. **116**, 10841, (2012).

(30) K. Sooklal, B. S. Cullum, S. M. Angel, and C. J. Murphy, Photophysical Properties of ZnS Nanoclusters with Spatially Localized Mn^{2+}, J. Phys. Chem. **100**, 4551 (1996)

(31) X. Zeng, J. Zhang, and F. Huang, Optical and magnetic properties of Cr-doped ZnS nanocrystallites, J. Appl. Phys., **111**, 123525 (2012)

(32) L. Brus, J. Phys., `Electronic Wavefunctions in Semiconductor Clusters, Chem. **90**, 2555 (1986)

(33) W. Chen, G. Li, J.-O. Malm, Y. Huang, R. Wallenberg, H. Han, Z. Wang, J.-O. Bovin, Pressure Dependence of Mn^{2+} Fluorescence in ZnS:Mn^{2+} Nanoparticles, J. Luminescence **91** 139 (2000)

(34) T.S. Moss, *Optical Properties of Semiconductors* (Academic Press, New York, 1959)

(35) N. Murase, R. Jagannathan,| Y. Kanematsu, M. Watanabe, A. Kurita, K. Hirata, T. Yazawa, and T. Kushida, Fluorescence and EPR characteristics of Mn^{2+}-doped ZnS nanocrystals prepared by aqueous colloidal method J. Phys. Chem. B, **103**, 754 (1999)

(36) M. Konishi, T. Isobe, M. Senna, Enhancement of photoluminescence of ZnS : Mn nanocrystals by hybridizing with polymerized acrylic acid, J. Luminescence **93**, 1 (2001)

(37) W. Chen, R. Sammynaiken, Y. Huang et al., Crystal field, phonon coupling and emission shift of Mn2+ in ZnS: Mn nanoparticles, J. Appl. Phys., **89**, 1120 (2001)

(38) T. Kushida, Y. Tanaka, Y. Oka, Absorption Spectra of Optically Pumped ZnS:Mn, J. Phys. Soc. Japan, **37,** 1341 (1974)

(39) Y. Xu and M.A.A. Schoonen, The absolute energy positions of conduction and valence bands of selected semiconducting minerals, American Mineralogist, **85**, 543 (2000)

(40) Y. R. Lee and A. K. Ramdas, Energy gap, excitonic, and ‘‘internal’’ Mn^{2+} optical transition in Mn-based II-VI diluted magnetic semiconductors, Phys. Rev. B, **38** 10600 (1988)

(41) Sapra, A. Prakash, A. Ghangrekar, N. Periasamy, and D.D. Sarma, Emission properties of manganese-doped ZnS nanocrystals, J. Phys. Chem. B, **109**, 1663 (2005)

Figures captions:

Fig. 1 (a) TEM image of ZnS:Mn (3 at.%) QDs prepared by laser ablation in water. Inset shows a magnified image of a QD. Circles are guide to the eyes. (b) Histogram of particle size distribution.

Fig. 2 XRD pattern of the ZnS:Mn (3 at.%) QDs prepared by laser ablation in water.

Fig. 3 Magnetic susceptibility versus temperature for ZnS:Mn (3 at.%) QDs prepared by laser ablation in water. Inset shows the inverse magnetic susceptibility vs temperature.

Fig. 4 Room temperature PL spectra of ZnS:Mn QDs of various Mn concentrations. 3 at.% sample was prepared by laser ablation and the rest by the co-precipitation method. Inset shows the PL of 0.5 at.% sample for clarity.

Fig. 5 PLE spectrum of ZnS:Mn (0.5 at.%) QDs prepared by the co-precipitation method. The spectrum was monitored at $\lambda = 610$ nm. Inset shows the absorption spectra for three samples (0, 0.5 and 5 at.%).

Fig. 6 Energy levels of Mn^{2+} ($3d^5$) ions in ZnS QDs (for particle diameter d = 3.2 nm) and that of Zn_2SnO_4.

Fig. 7 IPCE spectra of ZnS:Mn QDs of different Mn concentrations attached to Zn_2SnO_4 without ligands. 3 at.% sample was prepared by laser ablation and the rest by the co-precipitation method.

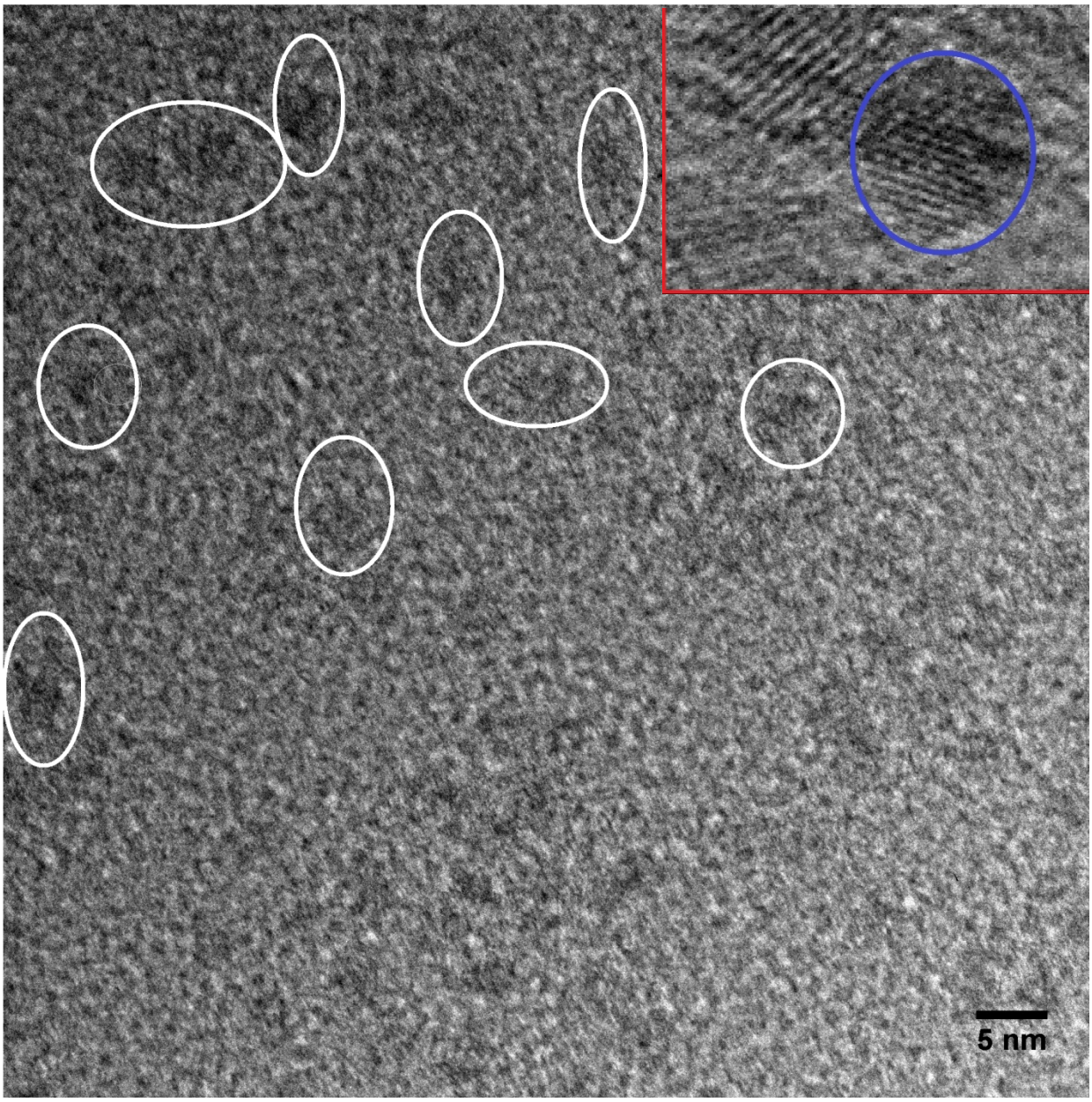

Fig. 1 (a)

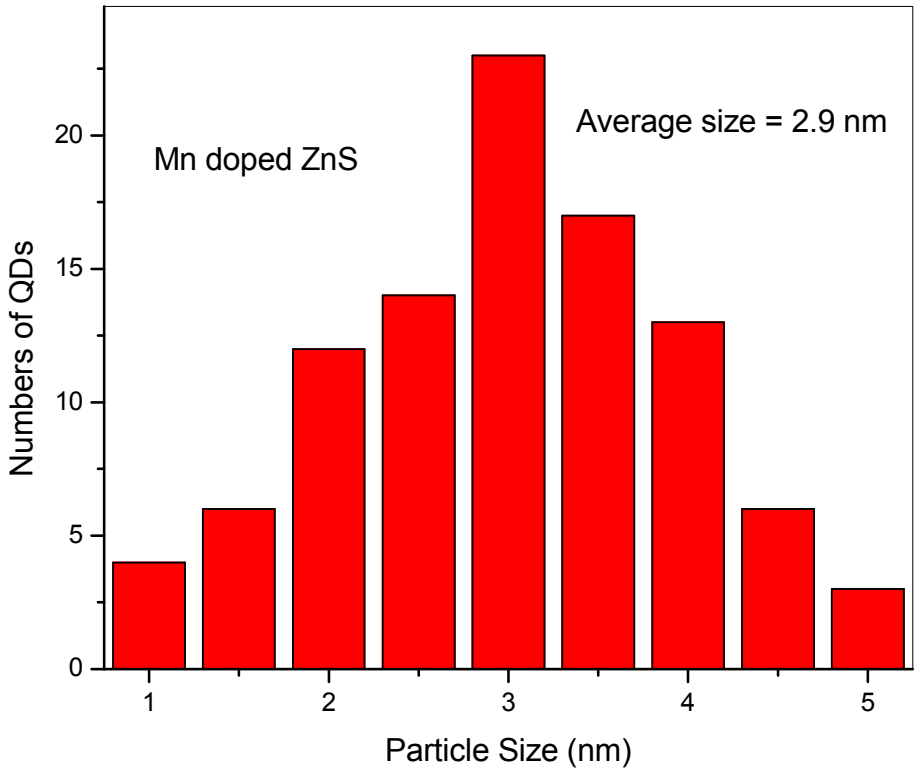
Mn doped ZnS
Average size = 2.9 nm
Numbers of QDs
0
5
10
15
20
1
2
3
4
5
Particle Size (nm)

Fig.1 (b)

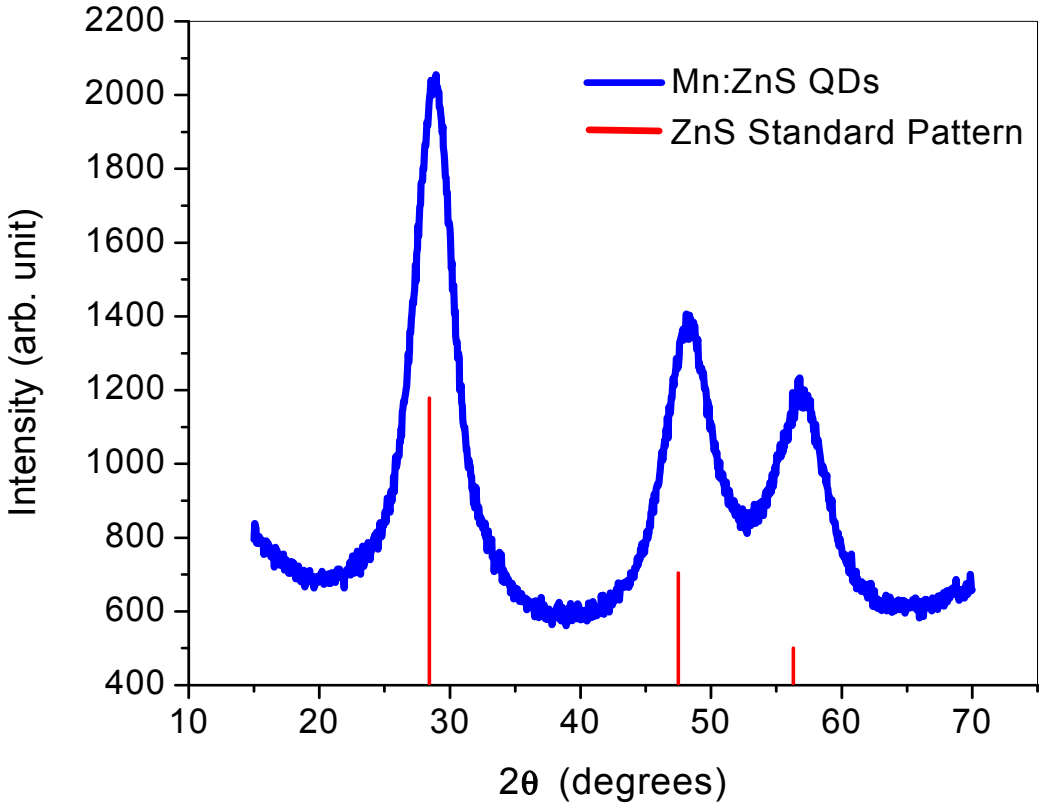
Mn:ZnS QDs
ZnS Standard Pattern
Intensity (arb. unit)
2θ (degrees)
2200
2000
1800
1600
1400
1200
1000
800
600
400
10
20
30
40
50
60
70

Fig. 2

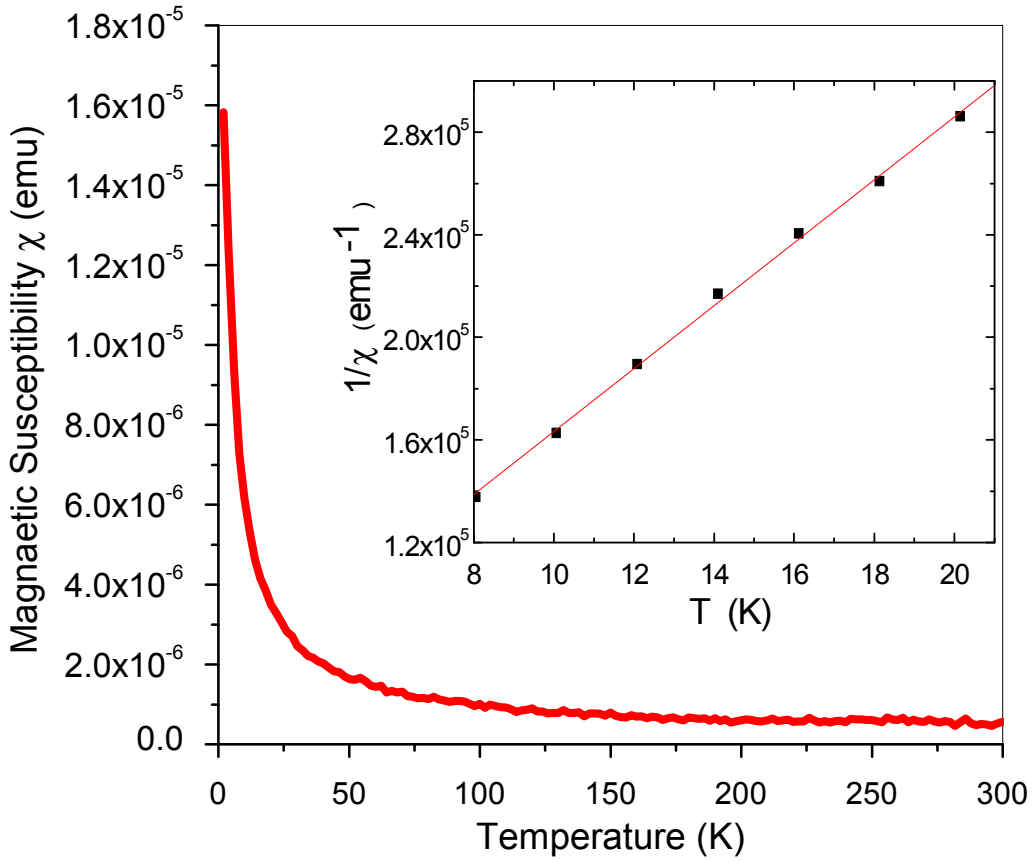
Magnaetic Susceptibility χ (emu)
1.8x10-5
1.6x10-5
1.4x10-5
1.2x10-5
1.0x10-5
8.0x10-6
6.0x10-6
4.0x10-6
2.0x10-6
0.0
0
50
100
150
200
250
300
Temperature (K)
1/χ (emu-1)
2.8x105
2.4x105
2.0x105
1.6x105
1.2x105
8
10
12
14
16
18
20
T (K)

Fig. 3

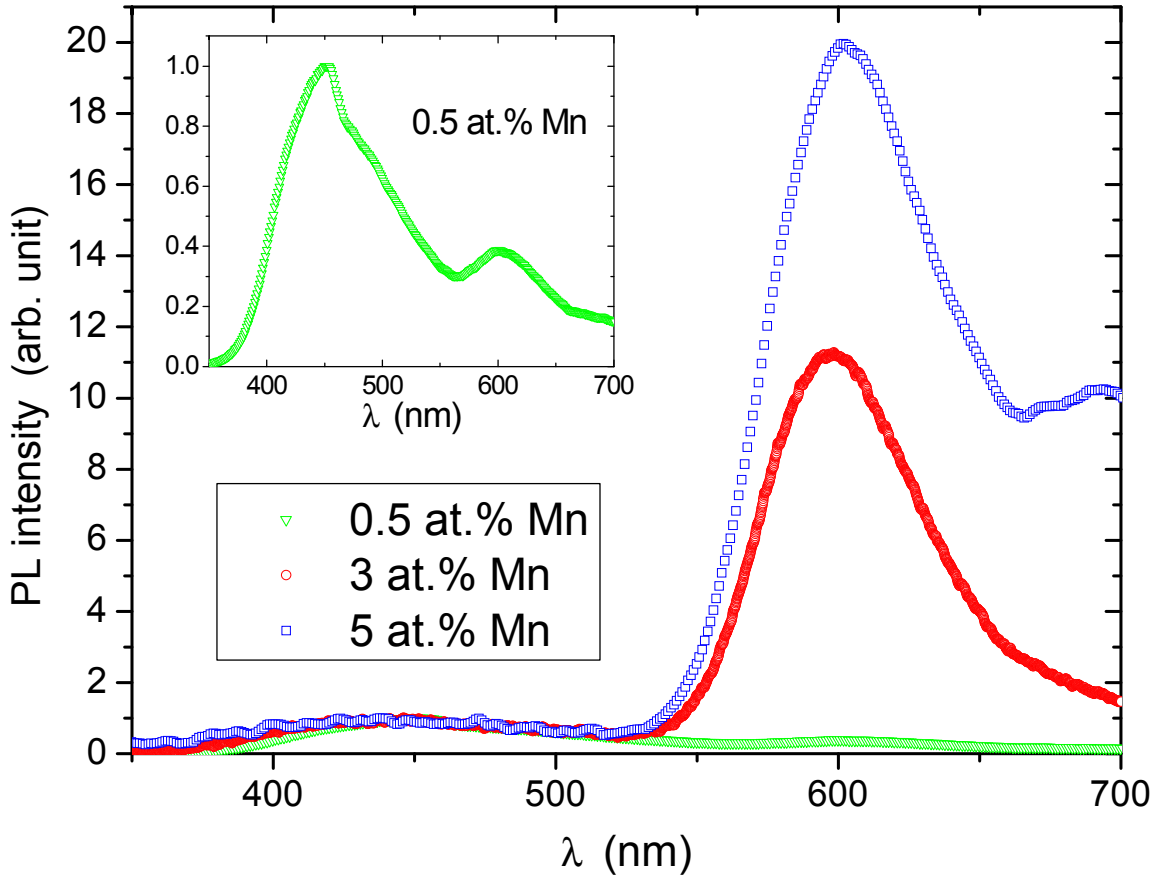

Fig. 4

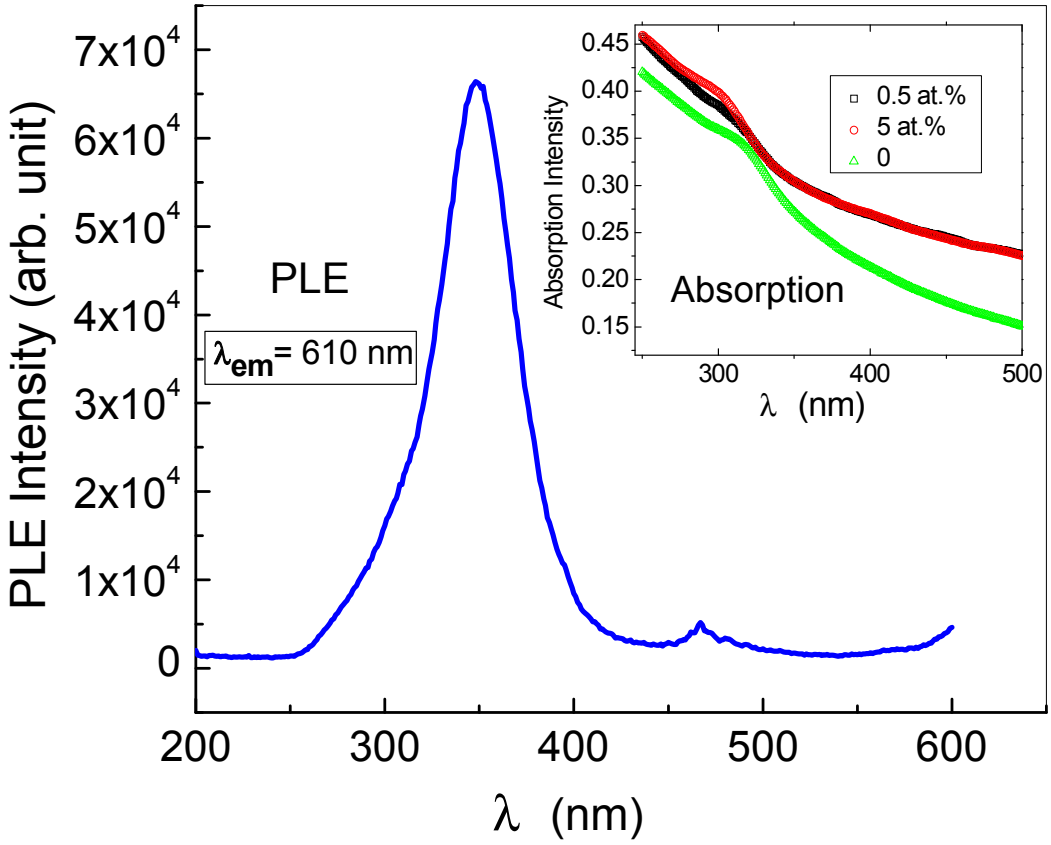
PLE Intensity (arb. unit)
7x10^4
6x10^4
5x10^4
4x10^4
3x10^4
2x10^4
1x10^4
0
200
300
400
500
600
λ (nm)
PLE
λem= 610 nm
Absorption Intensity
0.45
0.40
0.35
0.30
0.25
0.20
0.15
0.5 at.%
5 at.%
0
Absorption
300
400
500
λ (nm)

Fig. 5

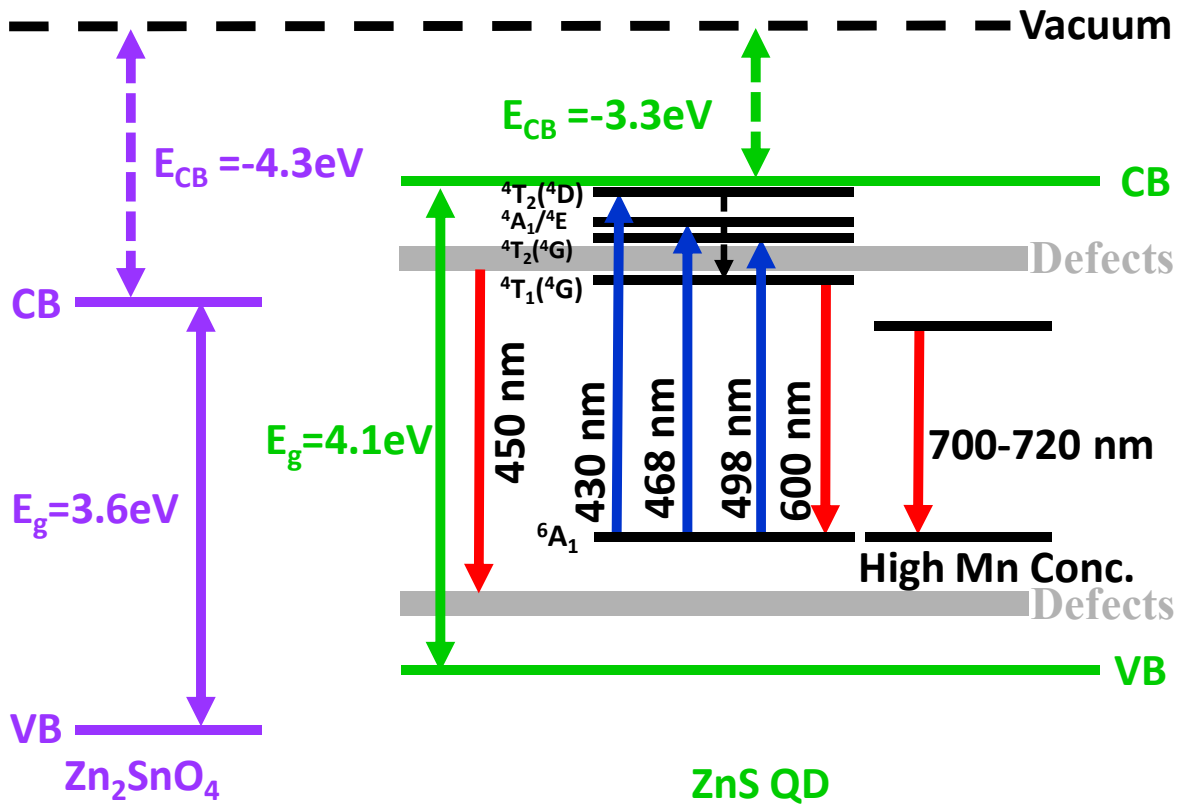
Vacuum
E_{CB} =-4.3eV
CB
E_g=3.6eV
VB
Zn_2SnO_4
E_{CB} =-3.3eV
CB
$^4T_2(^4D)$
$^4A_1/^4E$
$^4T_2(^4G)$
Defects
$^4T_1(^4G)$
E_g=4.1eV
450 nm
430 nm
468 nm
498 nm
600 nm
700-720 nm
$^6A_1$
High Mn Conc.
Defects
VB
ZnS QD

Fig. 6

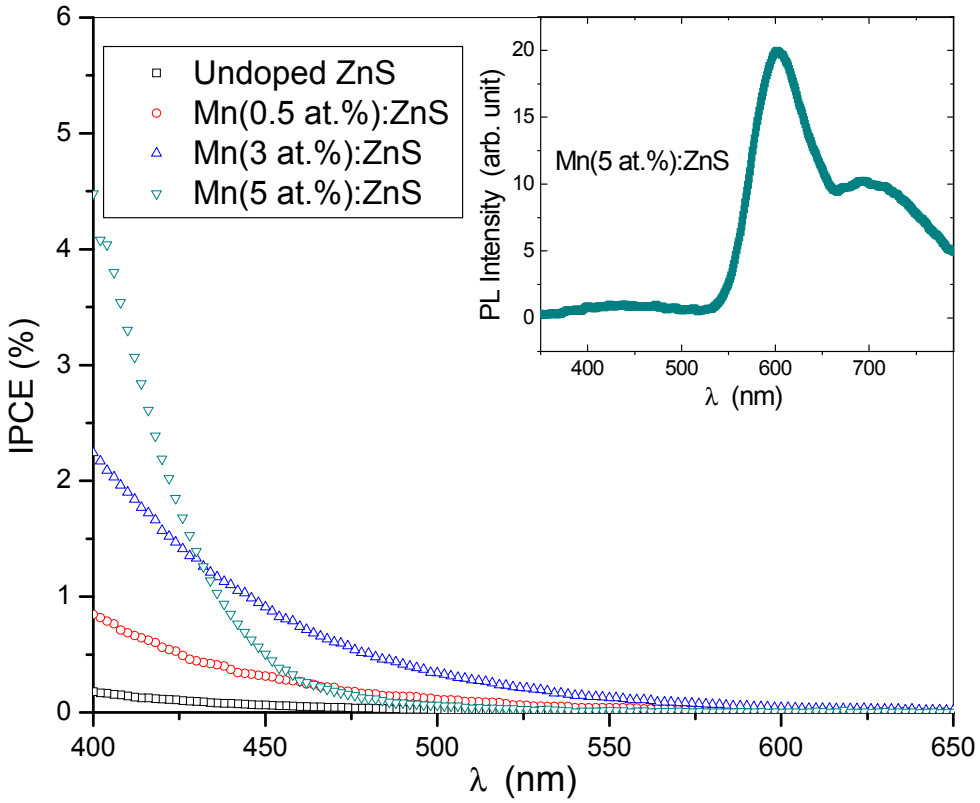
Undoped ZnS
Mn(0.5 at.%):ZnS
Mn(3 at.%):ZnS
Mn(5 at.%):ZnS
IPCE (%)
λ (nm)
PL Intensity (arb. unit)
Mn(5 at.%):ZnS
λ (nm)

Fig. 7